Inorganic Chemistry

Article

pubs.acs.org/IC

Bio-molecule Assisted Aggregation of $ZnWO_4$ Nanoparticles (NPs) into Chain-like Assemblies: Material for High Performance Supercapacitor and as Catalyst for Benzyl Alcohol Oxidation

Sivasankara Rao Ede,[†] Ananthakumar Ramadoss,[‡] U. Nithiyanantham,[†] S. Anantharaj,[†] and Subrata Kundu*[,†]

[†]Electrochemical Materials Science (ECMS) Division, CSIR-Central Electrochemical Research Institute (CECRI), Karaikudi-630006, Tamil Nadu, India

[‡]Nanomaterials and System Lab, Faculty of Applied Energy System, Science and Engineering College, Jeju National University, Jeju 690-756, Republic of Korea

Supporting Information

ABSTRACT: $ZnWO_4$ nanoparticles (NPs) that are assembled and aggregated together as chain-like morphology have been synthesized via the reaction of Zn(II) salt solution with sodium tungstate in the presence of the DNA scaffold under 5 min of microwave heating. The reaction parameters have been tuned to control the size of the individual particles and diameter of the chains. The significance of different reaction parameters and specific growth mechanism for the formation of particles is elaborated. The DNA-$ZnWO_4$ nanoassemblies have been used in two potential applications for the first time, namely, supercapacitor and catalysis studies. Supercapacitor study revealed that DNA-$ZnWO_4$ nanoassemblies exhibited good electrochemical properties having high specific capacitance value ~72 F/g at 5 mV s^{-1}, and electrodes possessed a good cyclic stability with more than 1000 consecutive times of cycling. Catalysis studies have been done for benzyl alcohol oxidation, and it was observed that DNA-$ZnWO_4$ nanoassemblies having smaller diameter gives better catalytic efficiency compared to other morphology. This is further authenticated from their BET surface area analysis. In the future, the self-assembled DNA-$ZnWO_4$ nanoassemblies could be a promising candidate for the synthesis of other mixed metal oxides and should be applicable in various emerging fields like Li ion batteries or photocatalysis, or as luminescent materials.

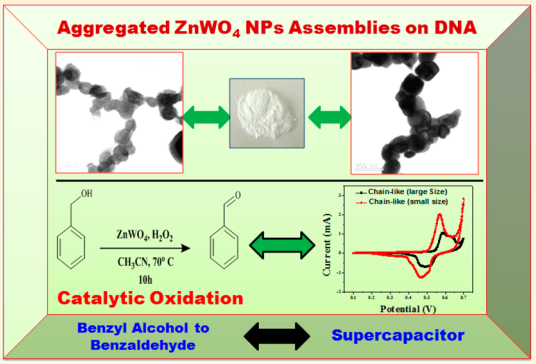

INTRODUCTION

The morphological synthesis and application of zero- and 1-dimensional (1-D) inorganic nanostructures are potentially important due to their unusual electronic, optical, and catalytic properties compared to those of their bulk counterparts.[1−3] While considering colloidal chemistry, the majority of reports have been employed to generate unidirectional nanomaterials of metals and semiconductors although materials like oxides or mixed metal oxides are poorly highlighted. Therefore, it is critical to find out a facile "bottom up" approach for the generation of 1-D self-assembled nanostructures within a short time scale. Apart from the synthesis point of view, another great challenge remaining is the generation of novel nanomaterial systems which can be economically affordable and ecofriendly for high-power energy related applications. In all the reported mixed metal oxides, the metal tungstates are significant due to their versatile chemical nature.[4] As reported, metal tungsten can be crystallized either in scheelite or in wolframite lattices.[4,5] Among the different tungstates, zinc tungstate ($ZnWO_4$) with wolframite structure has been of practical interest for a long time due to its magnetic,[6] scintillated,[7] luminescence,[8] photocatalytic,[9] and energy related[10] applications. The space and point group symmetries of monoclinic wolframite $ZnWO_4$ are $P2/c$ and C_{2h} respectively. The edge sharing ZnO_6 and WO_6 octahedra are making the finite zigzag chains of $ZnWO_4$ parallel to the [001] plane where the Zn and W atoms are paired with oxygen and displaced from the center of the octahedra by ~0.29 and 0.32 Å respectively.

Biomolecules like amino acids, proteins, and peptides have been used as potential templates for the generation of nanoscale materials.[11−13] Deoxyribonucleic acid (DNA) has been used as an important scaffold or template to grow nanostructures in specific morphology due to its various attractive physical and chemical properties. The negatively charged phosphate group and aromatic base molecules are the main candidates as binding sites through electrostatic interactions.[14−18] DNA templated assembly of coinage and Pt group metals,[14−18] semiconductor CdS,[19] and oxides like

Received: January 5, 2015
Published: April 6, 2015

DOI: 10.1021/acs.inorgchem.5b00018
Inorg. Chem. 2015, 54, 3851−3863

Fe_2O_3[20] and TiO_2[21] have been assembled for various applications.

Several methods have been utilized for the generation of $ZnWO_4$ nanomaterials, for example, sol−gel,[22] hydrothermal,[23] aqueous solution growth,[24] polymerized complex method,[25] solid state metathetic approach,[26] combustion method,[27] and so on. Kim et al. synthesized $ZnWO_4$ nanorods using a hydrothermal route and studied their applications for Li ion batteries.[10] Recently, Dhole et al. fabricated $ZnWO_4$ nanomaterials and used them for photocatalytic application for the reduction of methylene blue (MB).[28] Very recently Li et al. fabricated $ZnWO_4$ nanowall arrays grown over Ni foam using a hydrothermal route.[29] Compared to the conventional methods, microwave heating has specific advantages such as generation of higher reaction rates and reduced reaction time and energy due to its high penetration and concentrated power. Moreover, the microwave irradiation process can heat a reaction medium uniformly by generating homogeneous nucleation sites. We previously used microwave irradiation for the syntheses of Au,[30] Ag,[31] Os,[32] cobalt oxide,[33] and ZnO[34] nanomaterials within a very short time. Careful literature analysis revealed that the formation of self-assembled, aggregated $ZnWO_4$ NPs into chain-like assemblies on a DNA scaffold within 5 min of microwave heating has not been highlighted before. Moreover, the synthesized DNA-$ZnWO_4$ chain-like nanoassemblies are used as an anode material for supercapacitors and in organic catalysis studies.

Herein, we report the first ever synthesis of $ZnWO_4$ nanoparticles (NPs) that are assembled and aggregated together in chain-like morphology on a DNA scaffold using a simple microwave heating route within 5 min. $ZnWO_4$ nanoassemblies are synthesized via the reaction of $Zn(NO_3)_2 \cdot 6H_2O$ salt with $Na_2WO_4 \cdot 2H_2O$ in DNA scaffold by microwave heating. The ultimate diameter of the $ZnWO_4$ particles on DNA and length of the chains are controlled by tuning starting reagent concentrations and by varying the other reaction parameters. The DNA-$ZnWO_4$ aggregated nanoassemblies are utilized in two different potential applications: as suitable anode material in electrochemical supercapacitor studies and as a catalyst for benzyl alcohol oxidation. Supercapacitor study revealed that $ZnWO_4$ nanochains with different particle diameters showed different specific capacitance (C_s) values. The C_s value is followed as follows: chain-like (~small size) > (~large size). The higher C_s value of ~72 F/g at 5 mV s^{-1} has been observed for $ZnWO_4$ aggregated nanoassemblies having small size of the individual particles. The cyclic stability study indicates that the C_s value remains up to ~70% even after ~1000 times of cycling. From the catalysis study, it was observed that $ZnWO_4$ NPs having aggregated chain-like morphology acted as a catalyst for benzyl alcohol oxidation. In the current synthesis of $ZnWO_4$, DNA not only acts as capping agent but also helps to grow the synthesized particles in a specific morphology. Moreover, compared to other regular methods using commercial surfactants (such as CTAB, SDS, etc.), DNA is biocompatible and nontoxic in nature and has both reducing and stabilizing capability.

EXPERIMENTAL SECTION

Reagents. Deoxyribonucleic acid [double-stranded, herring testes, ~molecular weight ~50K bp (base pair)], zinc(II) nitrate, hexahydrate [$(Zn(NO_3)_2 \cdot 6H_2O$], and sodium tungstate, dihydrate ($Na_2WO_4 \cdot 2H_2O$) were bought from Sigma-Aldrich and used without further purification. Benzyl alcohol (99%, Alfa Aser), H_2O_2 (30%, S D Fine Chemicals limited), acetonitrile (CH_3CN, Rankem), and benzaldehyde (98%, Alfa Aser) were used as received. *N*-Methyl-2-pyrrolidinone (NMP), carbon black, polyvinylidene fluoride (PVDF), nickel foam, and potassium hydroxide were purchased from Alfa Aesar and used for supercapacitor studies. Deionized (DI) water was used for the synthesis and catalysis studies while Millipore water was used for electrochemical studies. The characterization details of $ZnWO_4$ nanoassemblies are given in the Supporting Information.

Microwave Syntheses of Aggregated $ZnWO_4$ NPs into Chain-like Assemblies on DNA Scaffold. $ZnWO_4$ nanoassemblies having aggregated chain-like morphology are synthesized via the reaction of zinc nitrate salt with sodium tungstate salt in the presence of DNA under microwave irradiation for 5 min. In the synthesis, 10 mL of DNA solution was mixed with 25 mL of 0.1(M) $Zn(NO_3)_2 \cdot 6H_2O$ salt with stirring. The solution became opaque after 10 min. After that 35 mL of DI water was added and stirred well for another 10 min. Then the container was put inside the microwave oven for 10 s; after that it was brought outside and 1 mL of $Na_2WO_4 \cdot 2H_2O$ solution (0.1M) was added with stirring. The same process was repeated several times to add 25 mL of $Na_2WO_4 \cdot 2H_2O$ solution. The total time taken for addition of all the $Na_2WO_4 \cdot 2H_2O$ solution was 250 s. The solution became white in color, microwave heating was continued for another 50 s, and then reaction was stopped. The container was taken out from the microwave oven and allowed to cool at room temperature (RT). The resultant white precipitate was processed by washing with ethanol and water and then dried at 60 °C. Then the material was annealed in a box furnace for ~2 h at different temperatures. The solid white mass was used for different spectroscopic and microscopic investigations as well as for supercapacitor and catalytic applications. Scheme 1 shows the schematic representation of $ZnWO_4$ nanoassemblies on DNA scaffold. The detailed concentrations of the reagent used, particle size and shape, and time of microwave heating for the generation of aggregated, chain-like $ZnWO_4$ nanoassemblies on the DNA scaffold are given in Table 1.

Scheme 1. Schematic Presentation of the Overall Preparation Process for the Formation of $ZnWO_4$ Aggregated, Chain-like Nanoassemblies

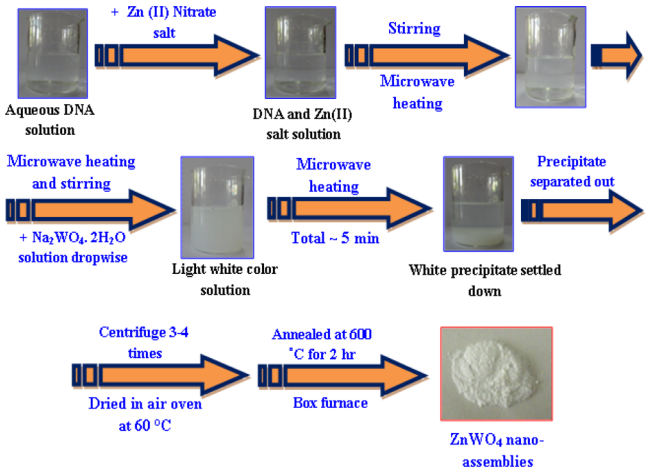

Electrode Fabrication for Supercapacitor Studies. As prepared $ZnWO_4$ nanomaterial was mixed with carbon black and polyvinylidene difluoride (PVDF) with the weight ratio of 80:10:10 in *N*-methylpyrrolidone (NMP) solvent for the preparation of working electrodes. The prepared mixture was then coated, pressed onto nickel foam, and then dried at 100 °C for 24 h. The loading mass of the electroactive material was about 3−4 mg cm^{-2}. Our electrochemical study consists of a standard three electrode system which includes the as prepared electroactive material as working electrode, platinum as counter electrode, and Ag/AgCl as the reference electrode. The whole study was carried out in 3 M KOH solution. Autolab electrochemical workstation was used to conduct the cyclic voltammetry (CV),

DOI: 10.1021/acs.inorgchem.5b00018
Inorg. Chem. 2015, 54, 3851−3863

Table 1. Detailed Final Concentrations of All the Reaction Parameters, Time of Reaction, and Particle Size and Shape

set no.	final concn (M)			time (min)		av particle size[a] (nm)	particle shape
	DNA	Zn(II) soln	$Na_2WO_4 \cdot 2H_2O$ soln	microwave heating	reaction		
1	1.34×10^{-4}	2.7×10^{-2}	2.7×10^{-2}	5	30	$L \sim 2-3$ μm, $D \sim 75 \pm 15$ nm	aggregated, chain-like (small size)
2	1.1×10^{-4}	2.7×10^{-2}	2.7×10^{-2}	5	90	$L \sim 1.2 \pm 0.3$ μm, $D \sim 120 \pm 15$ nm	aggregated, chain-like (larger size)

[a] L = length, D = diameter.

galvanostatic charge−discharge (GCD), and electrochemical impedance spectroscopy (EIS) measurements. An ac voltage with 5 mV amplitude in the 0.1 Hz to 100 kHz frequency range was applied to carry out EIS measurement at open circuit potential. The specific capacitances were calculated from CV and GCD curves according to the following equations:[21,35]

$$C_s = \frac{\int I(V)\, dv}{vm\Delta V} \quad (1)$$

$$C_s = \frac{I\Delta t}{m\Delta V} \quad (2)$$

where C_s is the specific capacitance (F g^{-1}), m indicates the mass of the electroactive material (g), v is the scan rate (V s^{-1}), ΔV is the voltage window (V), $\int I(V)\, dv$ is the integrated area under the CV curve loop (A V), I is the discharge current (A), and Δt is the discharge time (s).

Procedure for Catalytic Oxidation of Benzyl Alcohol to Benzaldehyde and Various Other Characterizations. The aggregated $ZnWO_4$ NPs assemblies were used for benzyl alcohol oxidation as a catalyst. In the reaction, 0.1 mL of benzyl alcohol was added with 10 mL of acetonitrile (as solvent) in a 15 mL glass vial. Then 0.1 g of $ZnWO_4$ powder and 1.8 mL of 30% H_2O_2 solution were introduced into the mixture and heated at 70 °C for about 10 h. The reaction vessel was covered tightly with aluminum foil to avoid the interference of atmospheric oxygen. A characteristic almond smell of benzaldehyde was observed, which indicated the completion of reaction. The confirmation of the final product was further confirmed by UV−vis, ^{1}H NMR, FT-IR, and HPLC studies. The aggregated $ZnWO_4$ NP assemblies were characterized using different spectroscopic tools, and the preparation of samples for those characterizations are given in detail in the Supporting Information.

RESULTS AND DISCUSSION

Transmission Electron Microscopy (TEM) and Energy Dispersive X-ray Spectroscopy (EDS) Analysis. Figure 1 shows the TEM images of $ZnWO_4$ particles aggregated in chain-like morphology on a DNA scaffold. The TEM images of chain-like $ZnWO_4$ nanoassemblies on DNA having smaller diameter of the chains at different magnification are shown in Figure 1a−c. Figure 1a,b shows the low magnification the TEM image where we can see that few chains are aggregated together to form a networklike structure. The image of a single chain is shown in Figure 1c. The average diameter of the chains is ∼75 ± 15 nm, and the average length of the chains is in the ∼2 to 3 μm range. The approximate lengths of the chains are calculated from TEM data using image J software. The individual particle size observed in the chains is ∼75 ± 5 nm. The selected area electron diffraction (SAED) pattern indicates that the particles are single crystalline in nature as shown in the inset of Figure 1c. The TEM images of $ZnWO_4$ nanochains where the diameter of the individual particles are large are shown in Figure 1d−f, respectively. From the low magnification TEM image (Figure 1d,f), we can see that a greater number of chains are assembling together. Figure 1f shows the TEM image containing only a single chain. The average diameter and nominal length of the chains are ∼120 ± 15 nm and ∼1.2 ± 0.3 μm, respectively. The average individual size of the particles is ∼115 ± 5 nm. The SAED pattern indicates that the particles are single crystalline in nature as seen in the inset of Figure 1f. From analyzing the TEM images in Figure 1, we understand that the individual $ZnWO_4$ particles are self-assembled and aggregated together and grown along the DNA to generate a chain-like morphology. Figure S-1 (Supporting Information) shows the EDS analysis of the synthesized $ZnWO_4$ nanoassemblies which consisted of various peaks originating from C, Ca, Si, Zn, W, and P; details are given in the Supporting Information.

UV−Vis Studies. UV−visible (UV−vis) absorption spectra of various solution mixtures utilized during the generation of aggregated $ZnWO_4$ NPs into chain-like assemblies on a DNA scaffold are shown in Figure 2, where curve a is the respective electronic spectrum of aqueous DNA solution with an intense band at ∼260 nm due to aromatic base molecules. The aqueous sodium tungstate solution (curve b, Figure 2) alone does not show any specific bands. Curve c in Figure 2 corresponds to the absorption band of an aqueous solution of zinc nitrate salt which has an intense band at ∼301 nm attributed to ligand to metal charge transfer spectra, which commonly appears for other d-block metal salts also.[3,30] A mixture of zinc nitrate salt with DNA shows a blue shift of the absorption band of zinc salt (itself) from ∼301 to 291 nm due to absorption of Zn^{2+} ions on DNA as seen in curve d, Figure 2. The specific absorption of metal cations with negatively charged DNA molecules and the shifting of absorption bands were observed earlier also. An immediate mixture of DNA, zinc nitrate salt, and sodium tungstate salt shows a small absorption hump at a wavelength range ∼244 to 300 nm as seen in curve e, Figure 2. It is interesting that the zinc salt, tungstate salt, and DNA peaks disappeared and a new broad peak appeared that might be due to the reaction of zinc salt with tungstate salt or their adsorption on DNA. Curves f and g show the excitonic absorption band of $ZnWO_4$ nanoassemblies on DNA. Curve f is the DNA-$ZnWO_4$ nanoassemblies having chain-like structure where the diameter of the chain is large. Curve g is the DNA-$ZnWO_4$ nanoassemblies also having chain-like structure although the diameter of the chain is small. From curve f, it is shown that the absorption peak maximum is located at ∼315 nm although the overall peak is broad, ranging from ∼279 to 470 nm. Similarly, for curve g, the peak maximum is located at ∼305 nm and the broad band extends from ∼271 to 500 nm. The shifting of peak maximum value toward the higher wavelength side is probably due to increase in particle sizes. It is noteworthy that the spectra in both f and g are taken in aqueous solution of $ZnWO_4$ after sonication for few minutes. We also collected the absorption spectra of the solid $ZnWO_4$ sample after making a thin film over the glass substrate given as

DOI: 10.1021/acs.inorgchem.5b00018
Inorg. Chem. 2015, 54, 3851−3863

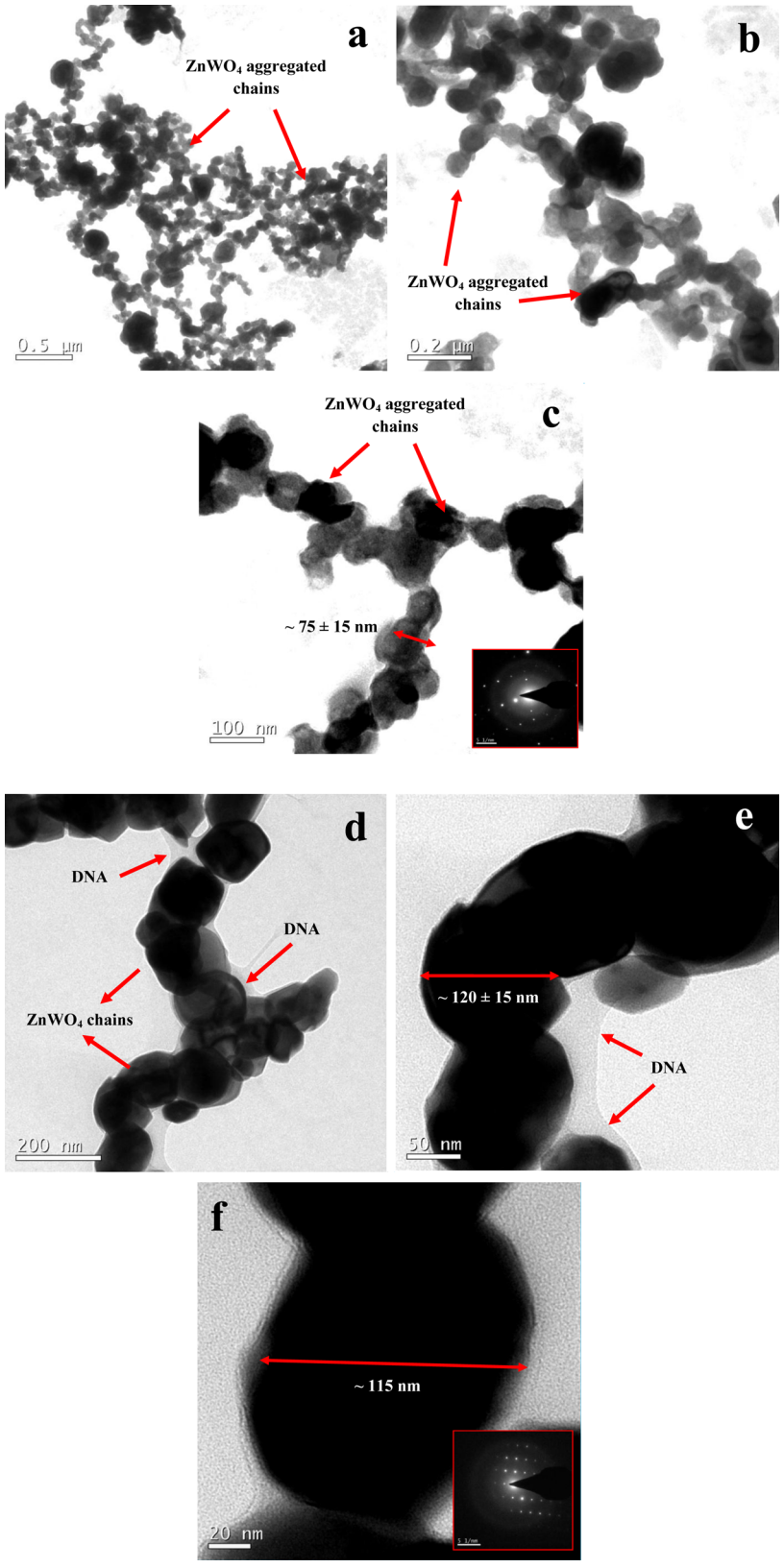

Figure 1. Transmission electron microscopy (TEM) image of the $ZnWO_4$ aggregated, chain-like nanoassemblies: panels a–c show the low and high magnified TEM image of $ZnWO_4$ chains having small size of the individual particles; panels d–f show the TEM image of the larger size $ZnWO_4$ particles. The insets of panels c and f show the corresponding selected area electron diffraction (SAED) patterns, which indicate that the particles are single crystalline in nature.

Figure S-2 (Supporting Information). The band gap energy of the $ZnWO_4$ thin film was evaluated from a photon energy ($h\nu$) dependent on $\alpha h\nu$ (Tauc plot)[36] from the given equation, $\alpha h\nu = (h\nu - E_g)^n$, where α, h, ν, and E_g are the absorption

DOI: 10.1021/acs.inorgchem.5b00018
Inorg. Chem. 2015, 54, 3851–3863

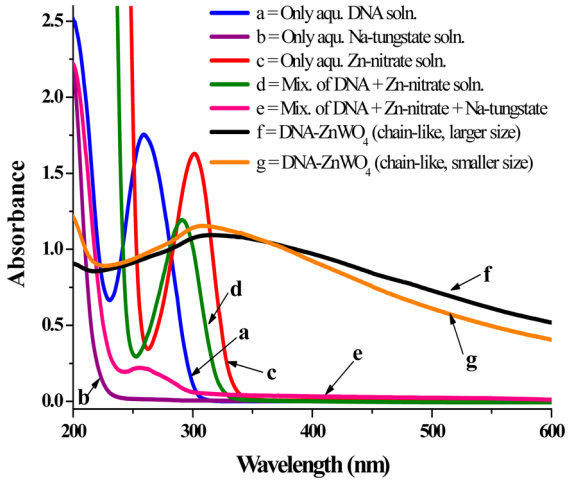

Figure 2. Room temperature (RT) UV−visible absorption spectra at the different stages of the synthesis process for the generation of $ZnWO_4$ aggregated, chain-like nanoassemblies on a DNA scaffold. Curve a shows the absorption band of only aqueous DNA solution; curve b shows the absorption band of aqueous sodium tungstate solution; curve c shows the absorption band of aqueous zinc nitrate salt solution; curve d shows the absorption band of a mixture of aqueous DNA solution and aqueous zinc nitrate solution; curve e shows the absorption band of a mixture of DNA, zinc nitrate salt, and sodium tungstate salt just after mixing; curve f and curve g show the excitonic absorption band of $ZnWO_4$ nanomaterials having chain-like morphology with large and small sizes of the individual particles, respectively.

coefficient, Planck constant, photon frequency, and photonic energy band gap, respectively. The parameter n corresponds to the types of electronic transitions taking place, where n is 1/2 for direct allowed and 2 for indirect allowed transitions. The reported value of n for $ZnWO_4$ is 1/2, and the reported band gap E_g for $ZnWO_4$ is 3.02 eV.[37] In our case the E_g value observed for the samples is 3.29 eV and the shifting of the band gap is attributed to the change in particle shape and size, respectively. The strong self-trapping tendency of the exciton formed via the O_{2p} hybridized W_{5d} state for W based semiconductors was reported earlier.[38] Similar types of band gap energy values were also reported for $ZnWO_4$ nanomaterials.[39]

X-ray Diffraction (XRD) Analysis. Figure 3 shows the XRD patterns of the aggregated $ZnWO_4$ NPs into chain-like assemblies at various reaction conditions. Figure 3A shows the four different XRD plots consisted together where the spectrum ran after annealing the samples at different temperatures. Curves a, b, c, and d are the XRD pattern at a annealing temperature of 200 °C, 300 °C, 400 °C, and 500 °C respectively. From the plots it is confirmed that, up to 400 °C, the material is purely amorphous and, above 400 °C, the phase is changing from amorphous to crystalline. At 500 °C, the sharp XRD peaks are observed of crystalline $ZnWO_4$ nanomaterials. The transformation of amorphous to crystalline phase occurred at nearly 500 °C. All the samples were annealed at 600 °C to get purely crystalline phase. Figure 3B shows two XRD plots (samples annealed at 600 °C) in which curve a is of DNA-$ZnWO_4$ chain-like assemblies having the smaller diameter and curve b is of the one with the larger diameter. Both of them are almost similar to one another and have peaks corresponding to the following planes: (010), (100), (011), (110), (−111), (020), (120), (200), (−121), (−112), (−211), (022), (220),

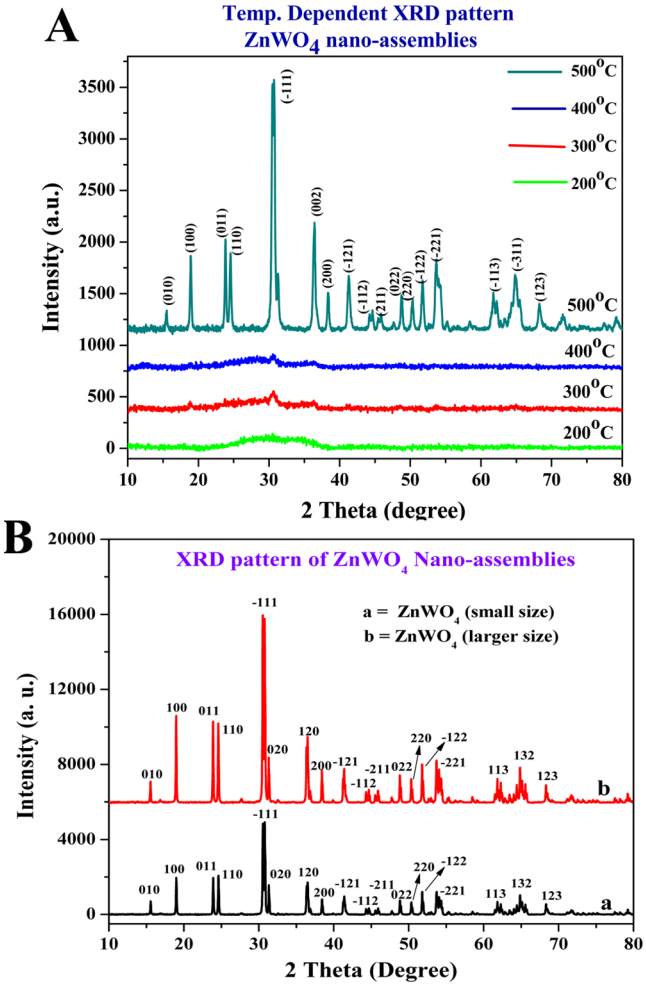

Figure 3. X-ray diffraction (XRD) pattern of the $ZnWO_4$ aggregated, chain-like nanoassemblies at various reaction conditions. Panel A shows the four different XRD patterns at an annealing temperature of 200 °C, 300 °C, 400 °C, and 500 °C respectively. Panel B shows two XRD patterns of the $ZnWO_4$ nanomaterials (annealed at 600 °C), where curve a denotes for small size chains and curve b denotes for the large size chains.

(−122), (−221), (113), (132), and (123) respectively. All the peaks are indexed with reference to the JCPDS card no. 15-0774 for pure $ZnWO_4$ with space group $P2/c$ and monoclinic wolframite phase.[10,28,29,39] The small full width at half-maximum (fwhm) reflection in the XRD pattern suggests a high degree of crystallinity in the final product. No broad peaks at lower 2θ range were observed, which revealed that there were no separate $ZnWO_4$ particles or excess DNA that also clearly indicated the purity of the synthesized DNA-$ZnWO_4$ samples.

X-ray Photoelectron Spectroscopic (XPS) Studies. Figure 4 is the XPS spectrum of the as prepared aggregated $ZnWO_4$ NPs into chain-like assemblies on a DNA scaffold. We have examined the morphology for the XPS spectrum although here we are showing the spectra for chain-like morphology having a small diameter of individual particles. Figure 4a is the XPS survey spectrum that shows various elements such as Zn, O, W, and C respectively of their specific binding energies. The Zn 2p, W 4f, and O 1s peaks are deconvoluted and fitted with background spectra as seen in Figures 4b, 4c, and 4d, respectively. The Zn $2p_{1/2}$ and Zn $2p_{3/2}$ peaks at high

DOI: 10.1021/acs.inorgchem.5b00018
Inorg. Chem. 2015, 54, 3851−3863

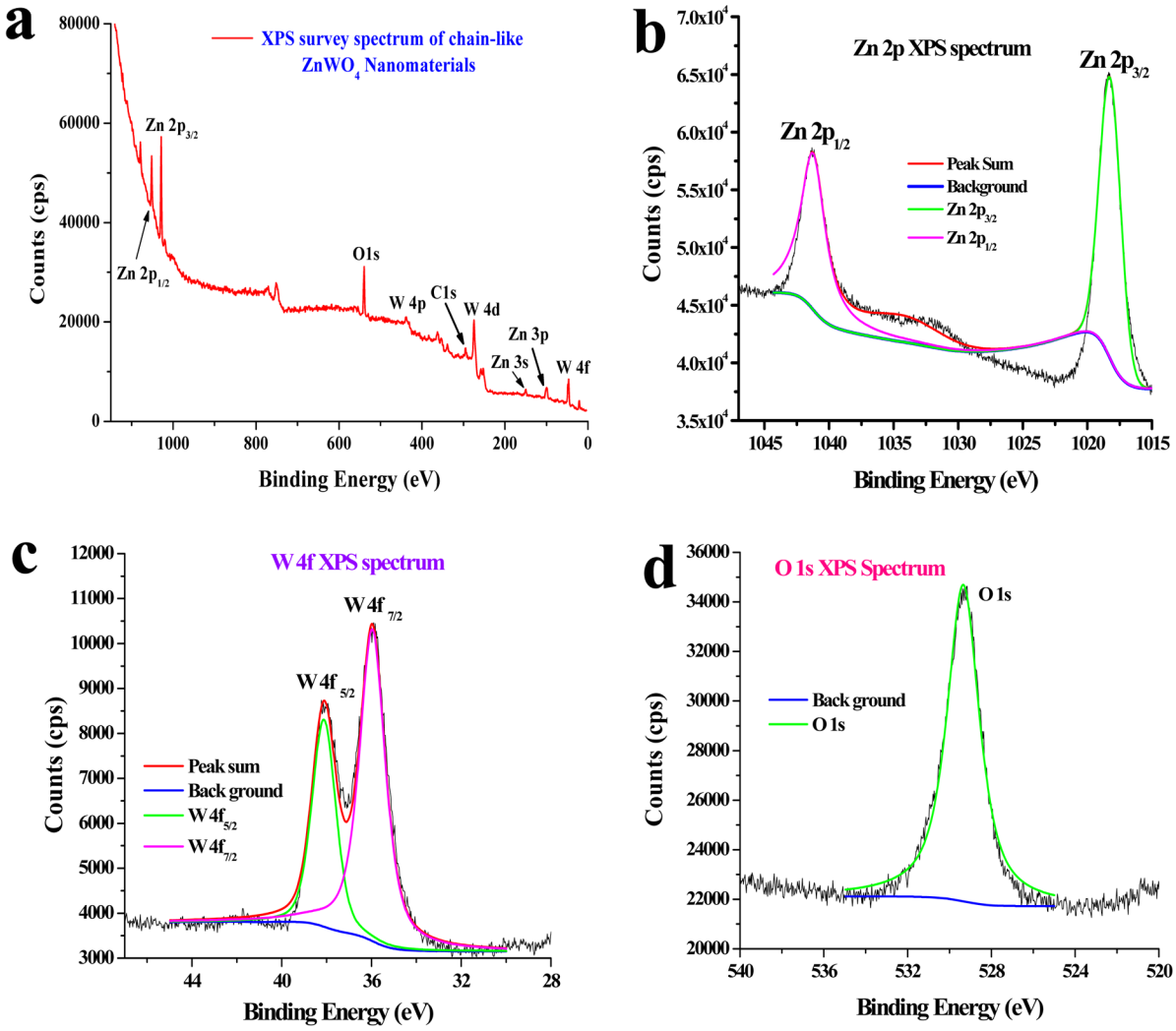

Figure 4. X-ray photoelectron spectroscopic (XPS) analysis of $ZnWO_4$ aggregated, chain-like nanoassemblies. Panel a shows the survey spectrum; panel b shows the high resolution scan for Zn 2p; panel c shows the high resolution scan for W 4f peaks; and panel d shows the high resolution scan for the O 1s XPS spectrum, respectively.

resolution scan at a binding energy of ~1041 eV and ~1018 eV are shown in Figure 4b. This splitting is due to spin orbit coupling of Zn 2p states. Similarly, the high resolution XPS spectrum of W 4f peaks is shown in Figure 4c. The W $4f_{7/2}$ and W $4f_{5/2}$ peaks appear at binding energies of ~35.9 eV and ~38.1 eV respectively. Figure 4d shows the O 1s XPS spectrum, and the peak appears at a binding energy of ~529.3 eV. Apart from Zn 2p, W 4f, and O 1s peaks in the survey spectrum (Figure 5a), a few other peaks like W 4p, W 4d, Zn 3s, and Zn 3p also appear. All these peaks at a specific binding energy clearly confirm the successful formation of $ZnWO_4$ nanomaterial.[40]

Photoluminescence (PL) Study. The photoluminescence (PL) emission spectra of aggregated $ZnWO_4$ NPs into chain-like assemblies on a DNA scaffold are shown in Figure S-3 (Supporting Information), which has an excitation wavelength of ~240 nm. Curve a shows the PL spectrum of the $ZnWO_4$ particles having smaller chain diameter, and curve b shows the PL emission spectrum having larger chain diameter. In both samples, apart from the sharp peak at 483 nm, the overall spectrum shows some broadening nature in the range 380 to 600 nm. It was reported that the blue and green emission originated from the intrinsic W_6^{6-} complex whereas the recombination of e−h pairs at oxygen atom deficient tungstate ions caused the yellow emission.[41,42] Our PL spectrum matches

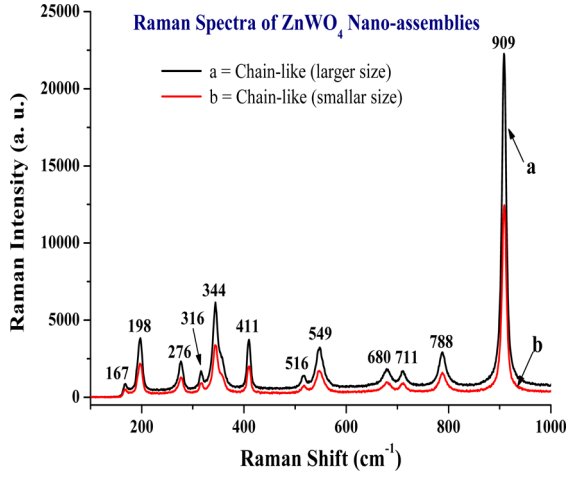

Figure 5. Laser Raman spectra of larger size (curve a) and smaller size (curve b) $ZnWO_4$ aggregated, chain-like nanoassemblies.

DOI: 10.1021/acs.inorgchem.5b00018
Inorg. Chem. 2015, 54, 3851−3863

nicely with previous reports.[41−43] The detailed discussion of PL study was elaborated in the Supporting Information.

Laser Raman and Thermal Analysis Study of the $ZnWO_4$ Nanoassemblies on DNA Scaffold. Figure 5, curve a and curve b show the laser Raman spectra of $ZnWO_4$ nanoassemblies of two different sizes on a DNA scaffold. The Raman spectra are taken using the sample annealed at 600 °C, which shows perfectly crystalline nature in XRD analysis. In curve a and curve b, the Raman bands are located in almost the same positions. Among the 36 lattice modes found by group theory analysis of monoclinic wolframite $ZnWO_4$ crystals, only 18 even vibrations ($8A_g + 10B_g$) are Raman active. In our present samples, the certain Raman bands appeared at 909 cm^{-1}, 788 cm^{-1}, 711 cm^{-1}, 680 cm^{-1}, 549 cm^{-1}, 516 cm^{-1}, 411 cm^{-1}, 344 cm^{-1}, 316 cm^{-1}, 276 cm^{-1}, 198 cm^{-1}, and 167 cm^{-1} respectively. All these Raman peaks confirmed the formation of $ZnWO_4$ nanomaterials.[10,44,45] The highest intense Raman bands are observed at a frequency line of 909 cm^{-1}, which is due to the stretching vibration of W−O bonds. At a low annealing temperature at 200 or 300 °C, the Raman peaks are not sharp but broad ended due to the amorphous nature of the samples. Thermogravimetric analysis (TGA) and differential thermal analysis (DTA) studies were carried out to investigate the crystallinity and thermal stability of the synthesized $ZnWO_4$ nanomaterials as shown in Figure S-4 (Supporting Information), curve a and curve b respectively. From the TGA curve, it was calculated that the % of weight loss after heating the samples up to 1000 °C is ∼1.69% where we had started our experiment with 5.91 mg of samples. No significant change was noticed in the DTA curve (curve b), although there is a broad exotherm observed at peak range 100 to 400 °C probably due to change in phase from amorphous to crystalline.[46,47] A detailed discussion regarding TGA-DTA analysis was elaborated in the Supporting Information.

FT-IR Analysis. The FT-IR spectra of only DNA and DNA encapsulated $ZnWO_4$ nanoassemblies are shown in Figure 6. Table S-1 (Supporting Information) shows the reported FT-IR bands[48] for DNA and the experimentally observed bands in our study and their corresponding band assignments. The FT-IR spectra are recorded at wavenumber scale 4000−400 cm^{-1}.

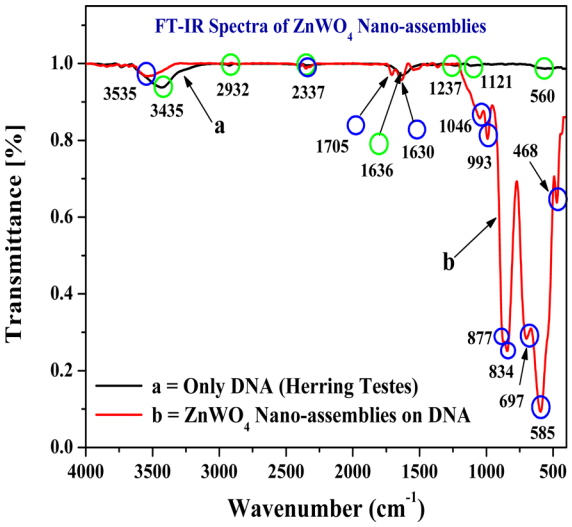

Figure 6. Fourier transform infrared (FT-IR) spectra of bare DNA (curve a) and DNA bound $ZnWO_4$ nanoassemblies (curve b) in the wavenumber range 400−4000 cm^{-1}.

Curve a and curve b denote the spectra for only DNA and DNA bound $ZnWO_4$ nanoassemblies, respectively. We are showing here the FT-IR spectrum of larger size $ZnWO_4$ nanoassemblies on a DNA scaffold. We also examined the other morphology, and that also exhibited similar types of spectra. We plot bare DNA spectra to make a comparison among them and to confirm the attachment of $ZnWO_4$ with DNA as well as to account for their specific interaction. For only DNA, a few specific peaks at 560 cm^{-1}, 1121 cm^{-1}, and 1237 cm^{-1} are observed that are originated from the deoxyribose region. The shift or disappearance of these specific peaks is noticed in case of DNA bound $ZnWO_4$ samples. In addition, there are a few other strong peaks also observed. There is a strong peak at ∼1636 cm^{-1} that is observed for only DNA attributed to the carbonyl group. In the case of DNA bound $ZnWO_4$, two peaks were observed at 1630 and 1705 cm^{-1} indicating the interaction of $ZnWO_4$ with DNA. In both samples there is a superimposed peak observed at 2337 cm^{-1} probably from the hydrocarbon stretching in DNA. In addition, another peak at 2932 cm^{-1} in both samples is due to the symmetric vibration of C−H bonds in the $-CH_2$ group. For only DNA sample, the OH stretching vibration is observed at 3435 cm^{-1} which is shifted to 3535 cm^{-1} in the case of DNA bound $ZnWO_4$ samples. Several high intense peaks are observed in the case of $ZnWO_4$ samples at the lower wavenumber side at 468 cm^{-1}, 585 cm^{-1}, 697 cm^{-1}, 834 cm^{-1}, 877 cm^{-1}, 993 cm^{-1}, and 1046 cm^{-1} which are fully absent in the case of only DNA. These bands are observed from the $ZnWO_4$ samples which match with the literature where the important peaks for $ZnWO_4$ appeared in the 450−1050 cm^{-1} region only. The bands at 468 and 585 cm^{-1} are assigned to the bending vibration W−O bonds. The peaks at 697 and 834 cm^{-1} correspond to the stretching vibration of W−O bonds. The Zn−O−W bonds show a strong peak at 877 cm^{-1} that is due to their bending and stretching deformation. For WO_6 and ZnO_6 octahedra, the symmetric and asymmetric deformation modes of W−O bonds and Zn−O bonds are observed at 473 and 430 cm^{-1} respectively.[48] All the above peaks were observed for our sample in the region 4000−400 cm^{-1}, which confirmed the successful formation of $ZnWO_4$ and their specific binding with DNA molecule.[28,39,49]

Mechanism of the Formation of Aggregated $ZnWO_4$ NPs into Chain-like Assemblies on a DNA Scaffold. DNA encapsulated aggregated $ZnWO_4$ NPs into chain-like assemblies of varying particle sizes are prepared via microwave heating for 5 min. The chain-like morphology with different diameters was formed at specific reagent concentrations as given in Table 1. From the control experiments, it was found that the presence of DNA is extremely important for the generation of aggregated, chain-like nanoassemblies. In the absence of DNA, the $ZnWO_4$ particles are formed but resulted as aggregated and agglomerated particles due to the absence of capping agents. Similarly, microwave heating also plays a specific role for the fast synthesis and uniform growth of small size $ZnWO_4$ particles on DNA. The same reaction using conventional heating took a longer time and resulted in mixed shaped, polydispersed and agglomerated particles. The most probable reaction for the formation of $ZnWO_4$ particles is given below:

$$Zn(NO_3)_2 \cdot 6H_2O + DNA \rightarrow DNA{-}Zn(NO_3)_2 \cdot 6H_2O \text{ complex}$$

DOI: 10.1021/acs.inorgchem.5b00018
Inorg. Chem. 2015, 54, 3851−3863

$$\text{DNA}-\text{Zn}(\text{NO}_3)_2\cdot 6\text{H}_2\text{O complex} + \text{Na}_2\text{WO}_4\cdot 2\text{H}_2\text{O} \rightarrow \text{DNA@ZnWO}_4\text{(nuclei)} + 2\text{NaNO}_3 + 8\text{H}_2\text{O}$$

$$\text{DNA@ZnWO}_4\text{ (nuclei)} \xrightarrow{\text{growth}} \text{DNA@ZnWO}_4\text{ (aggregated, chain-like assemblies)}$$

In the reaction, once the $ZnWO_4$ nuclei were formed, they grew along the DNA chain and resulted in the chain-like shape. From FT-IR analysis (Figure 6) also we observed that the deoxyribose sugar unit and the phosphate group were specifically bound with $ZnWO_4$ and directed their growth to chain-like shapes. From the UV−vis spectra in Figure 1, we have seen that the adsorption of Zn^{2+} ions to DNA takes place, which was confirmed via the shifting of individual absorption bands. Once the sodium tungstate salt was added, the WO_4^{2-} ions reacted with Zn^{2+} ions and generated the $ZnWO_4$ nuclei. The $ZnWO_4$ particles grow along the length of the DNA chain and generate the chain-like morphology. Scheme 2 shows the specific binding and formation of aggregated $ZnWO_4$ NPs into chain-like morphology on DNA scaffolds. From Scheme 2, we observed that Zn^{2+} ions were bound with DNA, and after feeding the WO_4^{2-} ions, they form $ZnWO_4$ nuclei and grow on the DNA chain to generate the chain-like morphology. Moreover, it was also depicted that, by varying DNA concentration, the diameter of the chains can also be controlled. Due to high DNA concentration, the initially formed chains were further agglomerated and formed the chains having larger diameter. In both cases the diameter of each $ZnWO_4$ particle was varied in the range of ~70 to 135 nm, and the overall diameter of the chains was also different. Our present mechanism is in good agreement with the one reported by Gao et al. for their specific generation of $BaWO_4$ nanowires on the DNA scaffold.[50] They observed that Ba^{2+} ions were directly bonded with adenine base of the DNA, and once WO_4^{2-} ions came in contact, they reacted and formed $BaWO_4$ and grew on the DNA to form $BaWO_4$ nanowires. In our present approach, we also assumed that a similar mechanism was taking place. During the direct bonding, we assumed that not all the sites of the DNA were bound to Zn^{2+} ions and the remaining area of the DNA was used for further growth, which proceeds through a multistep process. The $ZnWO_4$ nuclei then successfully grew in a preferential crystallographic direction, agglomerated, generated the large size $ZnWO_4$ particles, and finally stabilized on the DNA chain. In our current study, DNA was utilized as a stabilizing agent, which stabilized the synthesized $ZnWO_4$ NPs for their growth into chain-like morphology. We reported earlier the uniform growth of chain-like Au[51] and Ag[15] NPs on a DNA scaffold where DNA acted as reductant and stabilizer.[15,51] Two different sizes of aggregated DNA-$ZnWO_4$ nanoassemblies are used for the applications in supercapacitor and in catalysis studies as discussed below.

Scheme 2. Formation Mechanism and Binding of Zn(II) Ions to DNA for the Generation of Smaller and Larger Sizes of Aggregated, Chain-like $ZnWO_4$ Nanoassemblies

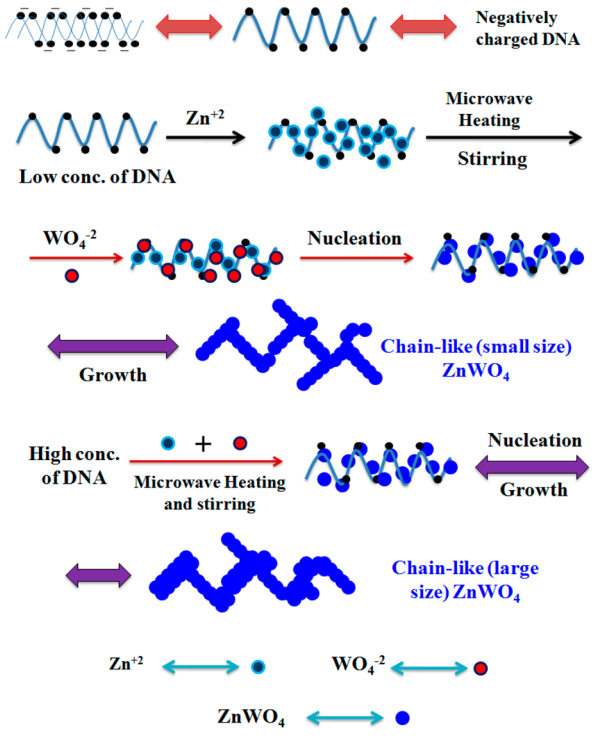

Electrochemical Supercapacitor Study Using DNA-$ZnWO_4$ Nanoassemblies. To investigate the pseudocapacitive behavior of the fabricated electrodes, a series of electrochemical measurements were carried out. First, electrochemical impedance spectroscopy (EIS) measurement was done to determine the conductive nature of the as-prepared electrode materials. The Nyquist plots of different sizes of $ZnWO_4$ electrodes are shown in Figure 7a. From both the curves in Figure 7a, a semicircle arc and a straight line were observed at the high- and low-frequency regions, respectively. The interfacial charge-transfer resistance (R_{ct}) occurring at the electrode/electrolyte interface and double layer capacitance (C_{dl}) is attributed to the semicircle arc at the high-frequency region.[52] The electrodes exhibit a negligible semicircle, suggesting a low charge transfer resistance and low interfacial resistance between current collector and electroactive material. In the low frequency region, the straight line of the slope of 45° represents the diffusive resistance (Warburg impedance) of the electrolyte ions in electroactive materials.[52] Both the electrodes were exhibiting a similar feature with a slope of 45°, indicating the more electrolyte ion diffusion to the electroactive materials. These results suggest the better conductivity and capacitive behavior of the as-fabricated electrode materials.

Furthermore, cyclic voltammetry (CV) and galvanostatic charge/discharge (GCD) measurements were done to evaluate the capacitive performance of as-prepared electrodes. Figure 7b displays the typical CV curves of two different sizes of $ZnWO_4$ electrodes at a scan rate of 5 mV s^{-1} within the potential window of 0.1 to 0.7 V. The CV curves indicate the presence of two redox peaks, which is probably due to the charge storage mechanism of $ZnWO_4$ originating from the faradaic redox reactions (pseudocapacitive behavior). Compared to larger size, the smaller size $ZnWO_4$ electrode shows higher integrated area, suggesting that the small size $ZnWO_4$ electrode has the highest energy storage capacity.

The kinetic irreversibility in the redox process due to polarization and ohmic resistance was evident by the shift observed in the cathodic and anodic peaks while changing the scan rate from 5 to 125 mV s^{-1} (Figure 7c) for the small size, aggregated $ZnWO_4$ chain-like electrode.[53,54] Further, the peak current increases obviously with increasing scan rate, demonstrating the good rate capability and better pseudocapacitive behavior. The specific capacitance is calculated from the

DOI: 10.1021/acs.inorgchem.5b00018
Inorg. Chem. 2015, 54, 3851−3863

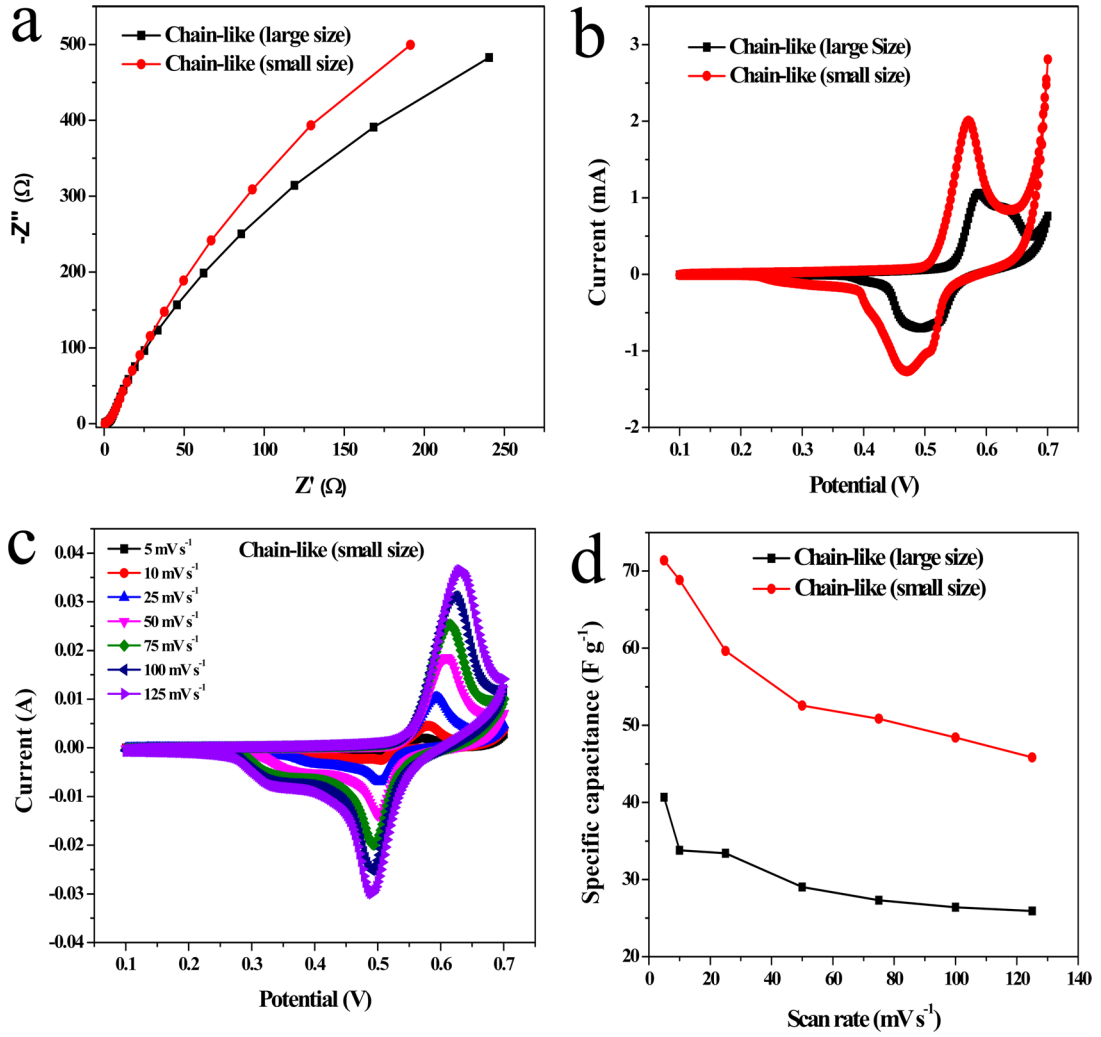

Figure 7. (a) Electrochemical impedance spectroscopy (EIS) and (b) cyclic voltammogram (CV) curves of small and large size $ZnWO_4$ electrodes. (c) CV curves of chain-like (small size) $ZnWO_4$ electrode at various scan rates. (d) Specific capacitance as a function of scan rate for small and large size chain-like $ZnWO_4$ electrodes.

CV curves using eq 1. The corresponding specific capacitance values calculated from CV curves at 5 mV s^{-1} of large and small size $ZnWO_4$ electrodes are 41 and 72 F g^{-1}. Figure 7d shows the specific capacitance of two different sizes of $ZnWO_4$ electrodes at varying scan rates where we observed higher specific capacitance for small size $ZnWO_4$ electrode compared to large size $ZnWO_4$ electrode at various scan rates. The enhanced specific capacitance of small size $ZnWO_4$ electrode is ascribed to their higher specific surface area, which provides a greater number of electroactive sites for charge storage. The observed BET surface areas were 155.15 and 164.21 m^2/g while the pore volumes were 0.571 and 0.551 cm^3/g for large and small size $ZnWO_4$ nanoassemblies, respectively. We perform the CV study with $ZnWO_4$ nanomaterials synthesized without DNA. We have seen that the observed capacitance value is much less compared to DNA-$ZnWO_4$ samples. This is probably due to their less BET surface area (135.49 m^2/g). The detailed values of DNA concentrations, pore volume, and surface area of our synthesized materials are elaborated in Table S-2 (Supporting Information). Moreover, the $ZnWO_4$ nanomaterial without DNA is not stable due to lack of specific stabilizing agent where the electrode material is peeling from the surface while running the CV experiment. The charge−discharge behaviors of two different sizes of $ZnWO_4$ electrodes were evaluated by galvanostatic charge−discharge tests in the potential window of 0.1 and 0.65 V at 0.4 mA cm^{-2}. As shown in Figure 8a, the nonlinear charge/discharge characteristics of both electrodes confirm the pseudocapacitance behavior. Further, the small size, aggregated chain-like $ZnWO_4$ electrode possesses the maximum charging/discharging time, resulting in the highest specific capacitance. This is in coincidence with the CV results. The GCD curves of small size $ZnWO_4$ electrode at different current densities are shown in Figure 8b. The voltage plateau observed from the GCD curves further confirms the pseudocapacitive nature and found good agreement with the CV peaks. Based on eq 2 the specific capacitance of two different sizes of aggregated chain-like $ZnWO_4$ electrodes was calculated to be 36 (large size) and 39 (small size) F g^{-1} at a current density of 0.2 mA cm^{-2}, respectively. Figure 8c is the plot of calculated specific capacitance and current density. The small size, aggregated, chain-like $ZnWO_4$ electrode exhibited higher specific capacitance, when compared to large size. The high capacitance for small size, aggregated, chain-like $ZnWO_4$ electrode can be attributed to the following points: (i) the small size, aggregated, chain-like nanostructure provides a high surface area for highly

DOI: 10.1021/acs.inorgchem.5b00018
Inorg. Chem. 2015, 54, 3851−3863

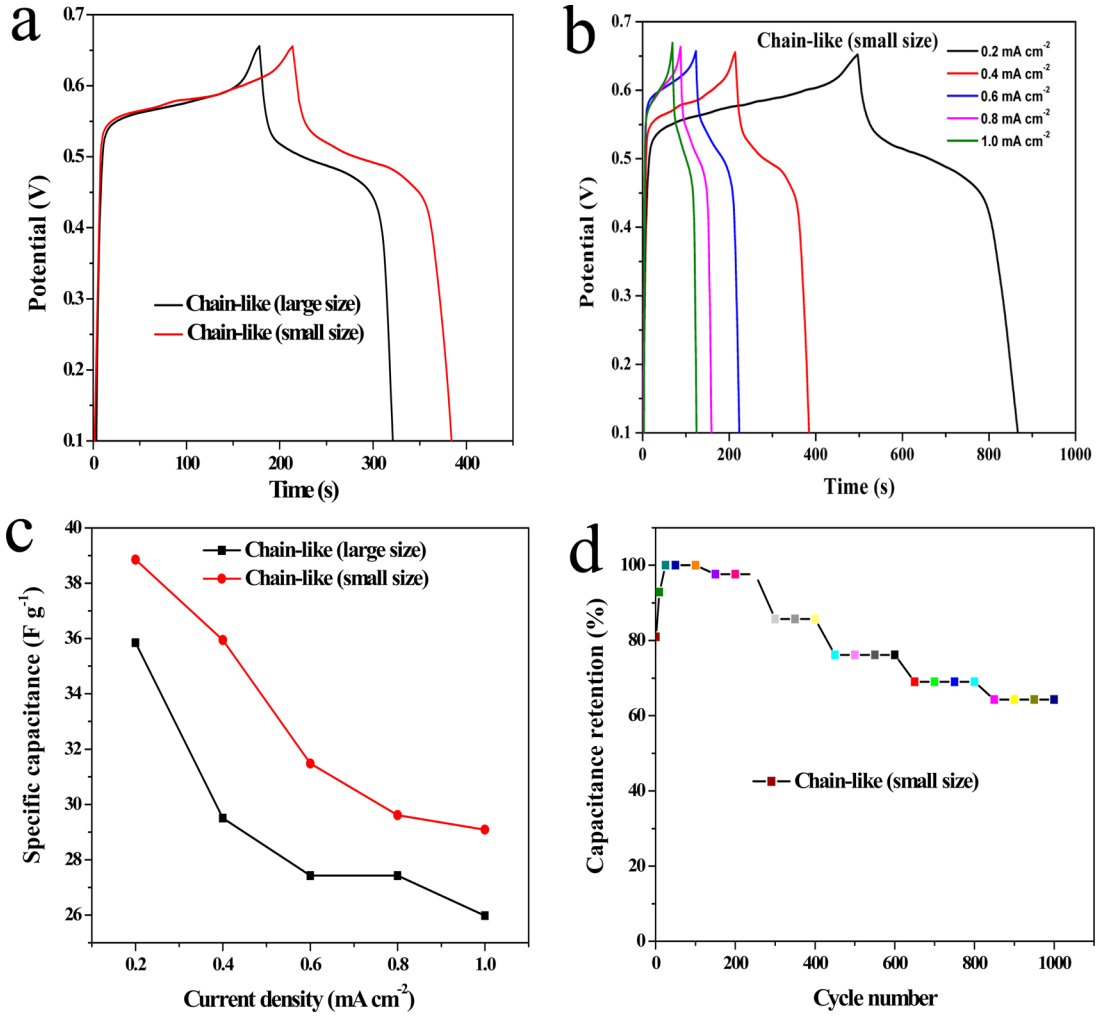

Figure 8. (a) Galvanostatic charge/discharge (GCD) curves of small and large size $ZnWO_4$ electrodes. (b) GCD curves of chain-like (small size) $ZnWO_4$ electrode at various current densities. (c) Specific capacitance of small and large size chain-like $ZnWO_4$ electrodes at different current densities. (d) Cyclic performance of small size chain-like $ZnWO_4$ electrode at 1 mA cm^{-2} for 1000 cycles.

feasible redox reactions; (ii) the smaller size, aggregated, chain-like nanostructure can significantly lower the diffusion path of electrolyte ions by facilitating fast ionic motion and redox reactions.

Long-term cyclic stability is an important parameter required for the practical applications of a supercapacitor. The GCD measurements were repeated for more than 1000 cycles to test the cyclic performance of small size chain-like $ZnWO_4$ electrode at a constant current density of 1 mA cm^{-2} in 3 M KOH solution (Figure 8d), which indicates a retention of 70% specific capacitance after 1000 cycles. This clearly implies the better cycling ability of the as-prepared small size chain-like $ZnWO_4$ electrode. In order to get further understanding into the rate capability, electrochemical impedance spectroscopy was performed on $ZnWO_4$ electrode before (Figure 9a) and after (Figure 9b) 1000 cycles. From Figure 9a and Figure 9b, it is understandable that the similarity observed in EIS spectra clearly indicates the better electrochemical stability of this electrode material. After 1000 cycles, a minute increase in resistance from 43 Ω to 49 Ω was observed and might be due to leaching of electroactive material coated over the electrode.[35]

Catalytic Oxidation of Benzyl Alcohol Using DNA-$ZnWO_4$ Nanoassemblies as Catalyst. The oxidation of alcohols plays a significant role in the organic syntheses as the

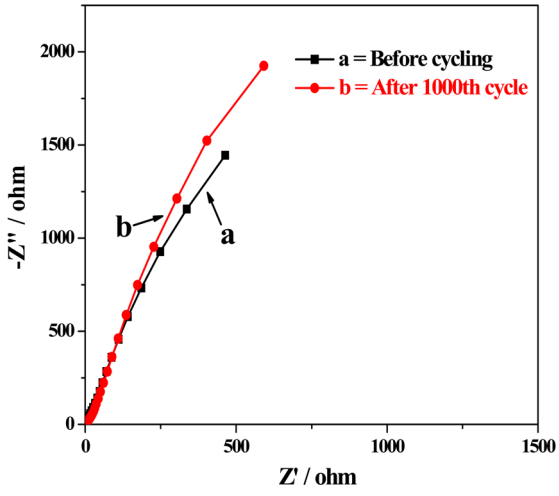

Figure 9. Nyquist plots of the $ZnWO_4$ electrode before (a) and after (b) 1000 cycles.

carbonyl compounds are widely used as intermediates both in industry and in laboratory.[55,56] However, the commercial production of carbonyl compounds involves the use of chromates and permanganates as oxidizing agents, which are

DOI: 10.1021/acs.inorgchem.5b00018
Inorg. Chem. 2015, 54, 3851−3863

expensive and toxic in nature.[57,58] Among all carbonyl compounds, the benzaldehyde is a key intermediate used extensively in perfumery, dye stuff, agrochemicals, and pharmaceutical industries. Recently our group reported the catalytic activity of metal and metal oxide NPs for application in specific organic reactions.[35,59] Up to now there are only several reports on the photocatalysis of various dyes using $ZnWO_4$ nanomaterials as catalyst.[60,61] In this study, for the first time we are focusing on the oxidation of benzyl alcohol to benzaldehyde using DNA-$ZnWO_4$ aggregated, chain-like nanoassemblies as catalyst. We have examined the oxidation reaction of benzyl alcohol in the presence of DNA-$ZnWO_4$ as catalyst using heterogeneous oxidation reaction in the presence of H_2O_2 as oxidizing agent and acetonitrile as solvent under 70 °C temperature. The feasible catalytic reaction takes place as

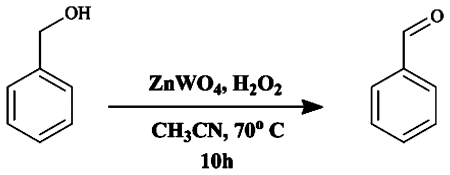

As discussed in the Experimental Section, about 0.1 mL of benzyl alcohol was added with 10 mL of acetonitrile followed by 0.1 g of $ZnWO_4$ powder and 1.8 mL of 30% H_2O_2 solution. The solution mixture was heated at 70 °C for 10 h. A characteristic almond smell of benzaldehyde confirmed the completion of reaction, which was further confirmed using UV−vis, ^{1}H NMR, FT-IR, and HPLC studies. In our catalysis reaction we conducted a couple of controlled experiments to check the influence of acetonitrile, DNA, and $ZnWO_4$ in the oxidation reaction. The reaction was carried out in the absence of $ZnWO_4$ catalyst but keeping other reaction parameters fixed. The reaction was examined with $ZnWO_4$ catalyst but in the absence of hydrogen peroxide. We also checked the solvent effect on the catalytic reaction, using water as solvent in place of acetonitrile, although a much smaller yield was obtained due to the partial solubility of benzyl alcohol in water. In all three cases, very poor or no catalysis reaction takes place. All these control experiments signified that the presence of all the reagents is extremely important to carry out the oxidation reaction. Instead of benzyl alcohol we also tested our catalysis reaction with similar types of compounds, such as geraniol and terpinol, which have allylic alcoholic groups, where we observed similar results. It is noteworthy that the overall catalysis reaction was performed using small size, aggregated, chain-like $ZnWO_4$ nanoassemblies as catalyst. The BET surface areas of the synthesized materials are given in the supercapacitor study section.

Figure 10A, curve a shows the UV−vis absorption spectra of benzaldehyde, and curve b shows the absorption spectra of benzyl alcohol. From curve a, the peak observed near 280 nm is due to the n−π* transition[62] of aldehyde group, the peak near 244 nm is due to the benzene ring, and the peak near 212 nm is due to the π−π* transition of the benzene ring. In curve b, the peak near 258 nm is due to the benzene ring and the peak near 221 nm is due to the π−π* transition of benzene ring. Here a new peak appeared at 280 nm due to aldehyde group that indicates the successful oxidation of benzyl alcohol to benzaldehyde. Figure 10B, curve a shows the FT-IR spectra of benzyl alcohol, and curve b shows the FT-IR spectra of benzaldehyde. In curve a, several peaks at 3419 cm^{-1}, 2317 cm^{-1}, 1633 cm^{-1}, 1454 cm^{-1}, 1379 cm^{-1}, and 1110 cm^{-1} were

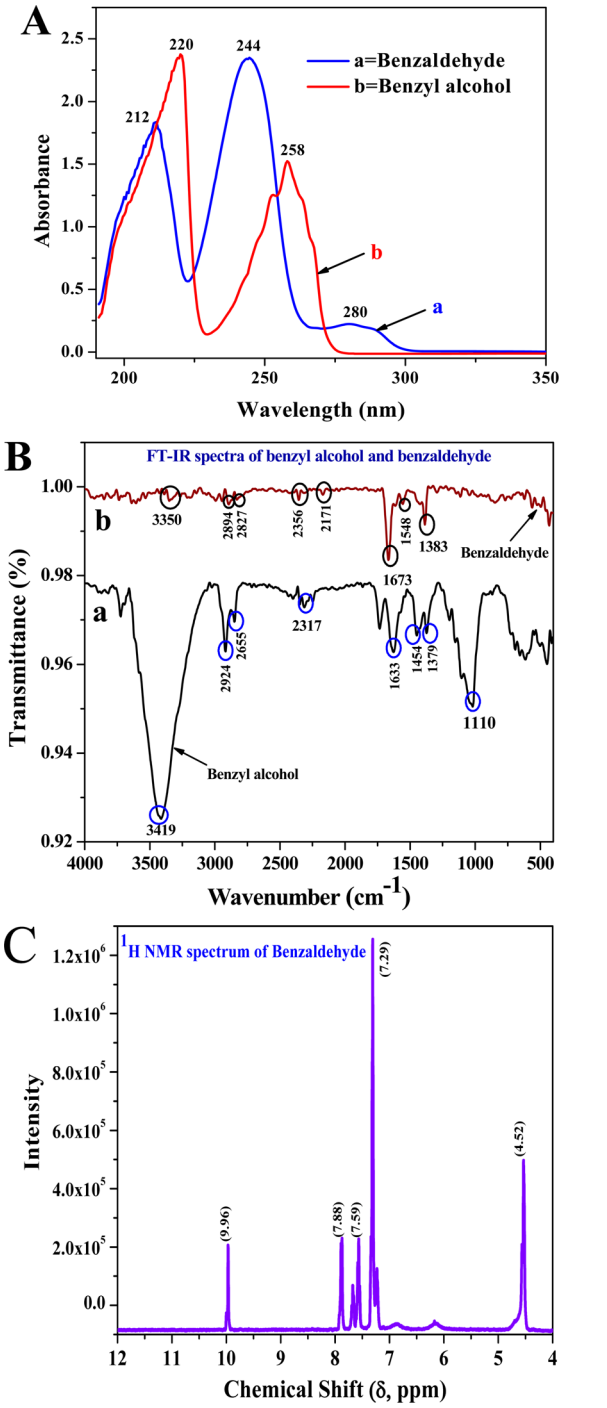

Figure 10. (A) Curve a shows the UV−vis absorption spectrum of benzaldehyde, and curve b shows the absorption spectrum of benzyl alcohol. (B) Curve a shows the FT-IR spectrum of benzyl alcohol, and curve b shows the FT-IR spectrum of benzaldehyde. (C) The ^{1}H NMR spectrum of benzaldehyde and acetonitrile mixture in $(CD_3)_2SO_4$ solvent.

observed. In curve b, peaks were observed at 3350 cm^{-1}, 2894 cm^{-1}, 2827 cm^{-1}, 2356 cm^{-1}, 2171 cm^{-1}, 1673 cm^{-1}, 1548 cm^{-1}, and 1383 cm^{-1} respectively. In curve b, the peak at 1673 cm^{-1} is attributed to C═O stretching, the peak at 2827 cm^{-1} is attributed to C−H stretching, and the peak at 1383 cm^{-1} is attributed to bending frequency of C−H group of aldehyde group which is absent in curve a. All the alcoholic peaks (in curve a) have disappeared in curve b, and the new peaks have

DOI: 10.1021/acs.inorgchem.5b00018
Inorg. Chem. 2015, 54, 3851−3863

appeared for aldehyde group, which indicates the oxidation of benzyl alcohol to benzaldehyde. Figure 10C shows the ^{1}H NMR spectrum of a benzaldehyde and acetonitrile mixture in $(CD_3)_2SO_4$ solvent. The singlet peak at 1.98 ppm is attributed to the $-CH_3$ group of acetonitrile (not shown here), the singlet at 3.32 is due to the interaction of $(CD_3)_2SO_4$ solvent (not shown here) with residual water, the peak at 4.52 ppm is due to residual water byproduct from hydrogen peroxide, the peaks in the range 7.29−7.89 ppm are due to deshielding of benzene protons by −CHO group, and the peak at 9.96 ppm is the characteristic of aldehyde proton which indicates the oxidation of benzyl alcohol to benzaldehyde.[63] The HPLC study was done with starting material and final product using methanol as solvent (figure not shown here). The rate of flow (R_f) value for starting material was 3.069 and for the final product was 3.343, which matches with reference benzaldehyde R_f value. From the chromatogram we calculated the yield and selectivity of our oxidation reaction. The yield was found to be nearly 70% with 100% selectivity. Apart from HPLC, we also did preliminary analysis using a gas chromatography mass spectroscopy (GC−MS) study. GC−MS analysis indicates that the spectrum of benzaldehyde shows a molecular ion peak at a m/z value of 106 $C_7H_6O^{+\bullet}$ and the characteristic peak for aldehyde group at a m/z value of 105 $C_7H_5O^{+\bullet}$, which indicate the removal of hydrogen from aldehyde group. As mentioned earlier, the yield and selectivity were already calculated from HPLC analysis, which nicely correlates with GC−MS analysis. We also conducted postreaction studies to check the recyclability of the catalyst and conducted the same reaction again and again for 10 consecutive times with the same catalyst by heating the catalyst every time up to 200 °C to remove the residues of previous reaction. It was found that, for up to 5−6 cycles, the catalytic behavior was not decreased much, although after that the time taken by the catalyst slowly increased cycle to cycle, which might be due to deactivation of the catalyst due to overoxidation of the active sites.[64,65] The potentiality of our DNA-$ZnWO_4$ aggregated, chain-like nanoassemblies as catalyst was compared with conventional reagents/catalysts. As there is no report of $ZnWO_4$ nanomaterial as catalyst for oxidation of benzyl alcohol, we compared our catalyst with other regents or other catalysts in a similar reaction.[66−69] The results are elaborated in Table S-3 (Supporting Information). We have seen that our present catalyst is much superior in terms of reaction temperature, product yield, and reaction selectivity.

CONCLUSION

In conclusion, aggregated $ZnWO_4$ NPs self-assembled into chain-like morphology were prepared via the reaction of Zn(II) salt solution with sodium tungstate solution in a DNA scaffold for 5 min of microwave heating. The morphology of the synthesized materials was tuned by varying the different reaction parameters. The roles of the DNA, microwave heating, and specific growth mechanism of the particle formation were examined in detail. The synthesized $ZnWO_4$ NPs aggregated into chain-like assemblies have been tested for the first time in two different applications, namely, electrochemical supercapacitor and organic catalysis reaction. It was seen that DNA-$ZnWO_4$ nanoassemblies exhibited good electrochemical properties with a high specific capacitance of ∼72 F/g at 5 mV s^{-1}. Among two morphologies, the higher C_s values are observed for small size, chain-like nanomaterials compared to large size. Moreover, the electrodes could maintain good cyclic stability over 1000 cycles. Apart from this, the material has been tested as catalyst for the oxidation of benzyl alcohol to benzaldehyde. Among the two different morphologies, smaller diameter of the individual particles gave better catalytic efficiency compared with larger size due to their higher BET surface area. In the future, the DNA-$ZnWO_4$ aggregated, chain-like nanoassemblies could be a promising candidate for the preparation of other nanomaterials and should be applicable in various emerging fields like Li ion batteries or photocatalysis, or as luminescent materials.

ASSOCIATED CONTENT

Supporting Information

Instrumental specifications and preparation of samples for various instrumental characterizations. Figures relevant to UV−vis, energy dispersive X-ray spectroscopy (EDS), photoluminescence (PL), and thermal analysis (TGA-DTA). Data for FT-IR analysis, BET analysis, and catalysis comparison (Tables S-1, S-2, and S-3, respectively). This material is available free of charge via the Internet at http://pubs.acs.org.

AUTHOR INFORMATION

Corresponding Author

*E-mail: skundu@cecri.res.in; kundu.subrata@gmail.com. Phone: (+ 91) 4565-241487. Fax: +91-4565-227651.

Notes

The authors declare no competing financial interest.

ACKNOWLEDGMENTS

S.K. wishes to acknowledge Dr. Vijayamohanan K. Pillai, Director, and Dr. M. Jayachandran, HOD, ECMS division, CSIR-CECRI, for their continuous support and encouragement. S.R.E. and S.A. wish to acknowledge Council of Scientific and Industrial Research (CSIR) for a JRF fellowship, and U.N. wishes to thank CSIR-CECRI for a research-intern fellowship. The institute start up funding (Project No. IHP 0067, DU No. 5, old number OLP-0067), support from the Central Instrumental Facility (CIF), and help from Mr. S. Radhakrishnan (NMR in-charge, CIF) and Mr. A. Rathishkumar (TEM in-charge, CIF), CSIR-CECRI, Karaikudi, are greatly appreciated.

REFERENCES

(1) Kundu, S.; Liang, H. *Adv. Mater.* **2008**, *20*, 826−831.
(2) Träger, F. *Appl. Phys. B: Lasers Opt.* **2001**, *73*, 291−429.
(3) Kundu, S.; Lau, S.; Liang, H. *J. Phys. Chem. C* **2009**, *113*, 5150−5156.
(4) Tilley, R. J. D. *Int. J. Refract. Met. Hard Mater.* **1995**, *13*, 93−109.
(5) Itoh, M.; Fujita, N.; Inabe, Y. *J. Phys. Soc. Jpn.* **2006**, *75*, 084705(1−8).
(6) Zhang, J.; Dong, L.; Lu, J.; Lan, H.; Sheng, C. *Chem. Mater.* **2002**, *14*, 4172−4177.
(7) Tan, G.; Zhang, L.; Wei, S.; Xia, A.; Ren, H. *Cryst. Res. Technol.* **2012**, *47*, 1279−1283.
(8) Vergados, J. D. *Phys. Rep.* **2002**, *361*, 1−56.
(9) Yu, S. H.; Liu, B.; Mo, M. S.; Huang, J. H.; Liu, X. M.; Qian, Y. T. *Adv. Funct. Mater.* **2003**, *13*, 639−647.
(10) Shim, H.-W.; Cho, I.-S.; Hong, K. S.; Lim, A.-H.; Kim, D.-W. *J. Phys. Chem. C* **2011**, *115*, 16228−16233.
(11) Scheibel, T.; Parthasarathy, R.; Sawicki, G.; Lin, X. M.; Jaeger, H.; Lindquist, S. L. *Proc. Natl. Acad. Sci. U.S.A.* **2003**, *100*, 4527−4532.
(12) Lee, S. W.; Mao, C. B.; Flynn, C. E.; Belcher, A. M. *Science* **2002**, *296*, 892−895.
(13) Mcmillan, R. A.; Paavola, C. D.; Howard, J.; Zaluzec, N. J.; Trent, J. D. *Nat. Mater.* **2002**, *1*, 247−252.

DOI: 10.1021/acs.inorgchem.5b00018
Inorg. Chem. 2015, 54, 3851−3863

(14) Kundu, S.; Liang, H. *Langmuir* **2008**, *24*, 9668−9674.
(15) Kundu, S. *Phys. Chem. Chem. Phys.* **2013**, *15*, 14107−14119.
(16) Kundu, S.; Wang, K.; Huitink, D.; Liang, H. *Langmuir* **2009**, *25*, 10146−10152.
(17) Seidel, R.; Ciacchi, L. C.; Weigel, M.; Pompe, W.; Mertig, M. *J. Phys. Chem. B* **2004**, *108*, 10801−10811.
(18) Monson, C. F.; Woolley, A. T. *Nano Lett.* **2003**, *3*, 359−363.
(19) Kundu, S.; Lee, H.; Liang, H. *Inorg. Chem.* **2008**, *48*, 121−127.
(20) Kinsella, J. M.; Ivanisevic, A. *J. Am. Chem. Soc.* **2005**, *127*, 3276−3277.
(21) Nithiyanantham, U.; Ramdoss, A.; Ede, S. R.; Kundu, S. *Nanoscale* **2014**, *6*, 8010−8023.
(22) Fu, H. B.; Lin, J.; Zhang, L. W.; Zhu, Y. F. *Appl. Catal., A* **2006**, *306*, 58−67.
(23) Zhou, J. H.; Chen, X. T.; Li, J.; Li, L. H.; Hong, J. M.; Xue, Z. L.; You, X. Z. *Chem. Phys. Lett.* **2003**, *375*, 185−190.
(24) Xiong, Y. J.; Xie, Y.; Li, Z. Q.; Li, X. X.; Gao, S. M. *Chem.—Eur. J.* **2004**, *10*, 654−660.
(25) Ryu, J. H.; Lim, C. S.; Auh, K. H. *Mater. Lett.* **2003**, *57*, 1550−1554.
(26) Parhi, P.; Karthik, T. N.; Manivannan, V. *J. Alloys Compd.* **2008**, *465*, 380−386.
(27) Dong, T. T.; Li, Z. H.; Ding, Z. X.; Wu, L.; Wang, X. X.; Fu, X. Z. *Mater. Res. Bull.* **2008**, *43*, 1694−1701.
(28) Garadkar, K. M.; Ghule, L. A.; Sapnar, K. B.; Dhole, S. D. *Mater. Res. Bull.* **2013**, *48*, 1105−1109.
(29) Guan, B.; Hu, L.; Zhang, G.; Guo, D.; Fu, T.; Li, J.; Duan, H.; Li, C.; Li, Q. *RSC Adv.* **2014**, *4*, 4212−4217.
(30) Kundu, S.; Peng, L.; Liang, H. *Inorg. Chem.* **2008**, *47*, 6344−6352.
(31) Kundu, S.; Maheshwari, V.; Niu, S.; Saraf, R. F. *Nanotechnology* **2008**, *19*, 65604−65609.
(32) Kundu, S.; Mukadam, M. D.; Yusuf, S. M.; Jayachandran, M. *CrystEngComm* **2013**, *15*, 482−497.
(33) Nithiyanantham, U.; Ede, S. R.; Kundu, S. *J. Mater. Chem. C* **2014**, *2*, 3782−3794.
(34) Kundu, S. *Colloids Surf., A* **2014**, *446*, 199−212.
(35) Ede, S. R.; Ramdoss, A.; Anantharaj, S.; Nithiyananatham, U.; Kundu, S. *Phys. Chem. Chem. Phys.* **2014**, *16*, 21846−21859.
(36) Tauc, J. *Mater. Res. Bull.* **1970**, *5*, 721−730.
(37) Leonard, K. C.; Nam, K. M.; Lee, H. C.; Kang, S. H.; Park, H. S.; Bard, A. J. *J. Phys. Chem. C* **2013**, *11*, 15901−15910.
(38) Nagirnyi, V.; Kirm, M.; Kotlov, A.; Lushchik, A.; Jonsson, L. *J. Lumin.* **2003**, *102*, 597−603.
(39) Huang, G.; Zhu, Y. *Mater. Sci. Eng., B* **2007**, *139*, 201−212.
(40) Huang, G.; Zhu, Y. *CrystEngComm* **2012**, *14*, 8076−8082.
(41) Blasse, G.; Lammers, M. J. J.; Robertson, D. S. *Phys. Status Solidi A* **1981**, *63*, 569−572.
(42) Grigorjeva, L.; Deych, R.; Millers, D.; Chernov, S. *Radiat. Meas.* **1998**, *29*, 267−271.
(43) Ovechkin, A. E.; Ryzhikov, V. D.; Tamulaitis, G.; Žukauskas, A. *Phys. Status Solidi A* **1987**, *103*, 285−290.
(44) Kalinko, A.; Kuzmin, A. *J. Lumin.* **2009**, *129*, 1144−1147.
(45) Siriwong, P.; Thongtem, T.; Phuruangrat, A.; Thongtem, S. *CrystEngComm* **2011**, *13*, 1564−1569.
(46) de Oliveira, A. L. M.; Ferreira, J. M.; Silva, M. R. S.; de Souza, S. C.; Vieira, F. T. G.; Longo, E.; Souza, A. G.; Santos, I. M. G. *J. Therm. Anal. Calorim.* **2009**, *97*, 167−172.
(47) Nithiyanantham, U.; Ede, S. R.; Kesavan, T.; Raghupati, P.; Mukadam, M. D.; Yusuf, S. M.; Kundu, S. *RSC Adv.* **2014**, *4*, 38169−38181.
(48) Banyay, M.; Sarkar, M.; Graslund, A. *Biophys. Chem.* **2003**, *104*, 477−488.
(49) Fomichev, V. V.; Kondratov, O. I. *Spectrochim. Acta* **1994**, *50A*, 1113−1120.
(50) Li, N.; Gao, F.; Hou, L.; Gao, D. *J. Phys. Chem. C* **2010**, *114*, 16114−16121.
(51) Kundu, S.; Maheshwari, V.; Saraf, R. F. *Langmuir* **2008**, *24*, 551−555.
(52) Fan, Z.; Yan, J.; Wei, T.; Zhi, L.; Ning, G.; Li, T.; Wei, F. *Adv. Funct. Mater.* **2011**, *21*, 2366−2375.
(53) Luo, W.; Hu, X.; Sun, Y.; Huang, Y. *J. Mater. Chem.* **2012**, *22*, 8916−8921.
(54) Meher, G. S. K.; Rao, R. *J. Phys. Chem. C* **2011**, *115*, 15646−15654.
(55) Pillai, U. R.; Sahle-Demessie, E. *J. Mol. Catal. A: Chem.* **2003**, *191*, 93−100.
(56) Hudlicky, M. *Oxidations in Organic Chemistry*; American Chemical Society: Washington, DC, 1990.
(57) Lee, D. G.; Spitzer, U. A. *J. Org. Chem.* **1970**, *35*, 3589−3590.
(58) Merger, F. M.; Lee, C. *Tetrahedron Lett.* **1981**, *22*, 1655−1656.
(59) Anantharaj, S.; Nithiyanantham, U.; Ede, S. R.; Kundu, S. *Ind. Eng. Chem. Res.* **2014**, *53*, 19228−19238.
(60) Huang, G.; Zhu, Y. *Mater. Sci. Eng., B* **2007**, *139*, 201−208.
(61) Shi, R.; Wang, Y.; Li, D.; Xu, J.; Zhu, Y. *Appl. Catal. B* **2010**, *100*, 173−178.
(62) Caralp, F.; Foucher, V.; Lesclaux, R.; Walungton, T. J.; Hurley, M. D. *Phys. Chem. Chem. Phys.* **1999**, *1*, 3509−3517.
(63) Shaabani, A.; Mirzaei, P.; Naderi, S.; Lee, D. G. *Tetrahedron* **2004**, *60*, 11415−11420.
(64) Vandam, H. E.; Wisse, L. J.; Vanbekkum, H. *Appl. Catal.* **1990**, *61*, 187−197.
(65) Mallat, T.; Baiker, A. *Chem. Rev.* **2004**, *104*, 3037−3058.
(66) Harding, K. E.; May, L. M.; Dick, K. F. *J. Org. Chem.* **1975**, *40*, 1664−1665.
(67) Dimitratos, N.; Lopez-Sanchez, A. J.; Morgan, D.; Carley, A.; Prati, L.; Huthings, G. J. *Catal. Today* **2007**, *122*, 317−324.
(68) Alhumaimess, M.; Lin, Z.; He, Q.; Lu, L.; Dimitratos, N.; Dummer, N. F.; Conte, M.; Taylor, S. H.; Bartley, J. K.; Kieyl, C. J.; Huthings, G. J. *Chem.—Eur. J.* **2014**, *20*, 1701−1710.
(69) Pina, C. D.; Falletta, E.; Rossi, M. *J. Catal.* **2008**, *260*, 384−386.

DOI: 10.1021/acs.inorgchem.5b00018
Inorg. Chem. 2015, 54, 3851−3863